arXiv:cond-mat/0111364v1 [cond-mat.stat-mech] 20 Nov 2001

Spatio-temporal log-stable process for the turbulent energy-cascade

Jürgen Schmiegel[a+b] and Martin Greiner[a+c]
[a] *Max-Planck-Institut für Physik komplexer Systeme, Nöthnitzer Str. 38, D–01187 Dresden, Germany*
[b] *Department of Physics, University of Stellenbosch, 7600 Stellenbosch, South Africa*
[c] *Department of Physics, Duke University, Durham, NC 27708, USA*
(1.11.2001)

We present a dynamical log-stable process for the spatio-temporal evolution of the energy-dissipation field in fully developed turbulence. The process is constructed from multifractal scaling relations required for two-point correlators of arbitrary order. n-point correlation functions are calculated analytically and interpreted in terms of generalised fusion rules and in terms of the random multiplicative cascade picture. Multiplier distributions are compared with experimental results.

PACS: 47.27.Eq, 05.40.-a, 02.50.Sk
KEYWORDS: fully developed turbulence, multifractality, n-point correlations, multiplier distributions, stable distributions.

CORRESPONDING AUTHOR:
Jürgen Schmiegel
MPIPKS
Nöthnitzer Str. 38
Dresden 01187
tel.:+49 (351) 871-1217
fax: +49 (351) 871-1999
email: schmiego@mpipks-dresden.mpg.de

I. INTRODUCTION

The large number of strongly-coupled many-scales degrees of freedom in fully developed turbulent flows renders any analytical and computational approach impractical for very high Reynolds numbers. An alternative avenue is to look for a statistical description [1] which by itself presents a difficult task. Only a few rigorous results, as for example the 4/5-law [2,3], have been derived from the underlying Navier-Stokes equation, employing some idealised assumptions like homogeneity, isotropy, etc. On the other hand, a multitude of empirical facts are known from the experimental analysis [4], giving rise to a huge playground for phenomenological modelling [3,5].

One such class of data-driven models are random multiplicative cascade processes ($RMCP$) [3], which are motivated by Richardsons energy cascade picture [6]. They emphasise the observed multifractal nature of turbulent fields by assigning independent and identically distributed random weights q_j to a nested hierarchy of inertial range scales $\eta \leq l_j = L/\lambda^j \leq L$, confined by the integral scale L and the dissipation length scale η. Amplitudes $\Pi_j = q_1 \cdots q_j$ of the energy-flux density field at intermediate scales l_j are then given as a multiplication of random weights, so that their respective moments

$$\left\langle \Pi_j^n \right\rangle = \langle q^n \rangle^j = \left(\frac{L}{l_j} \right)^{\tau_n} \tag{1}$$

indicate multiscaling. Note that interpretationally the energy flux field $\Pi(x)$ is set equal to the energy-dissipation field $\epsilon(x)$ and that experimentally Π_j is identified with the coarse grained surrogate energy-dissipation field $\epsilon_j = l_j^{-1} \int_{l_j} \epsilon(x) dx$. As a consequence of the scaling (1), two-point correlations

$$\langle \epsilon(x_1)^{n_1} \epsilon(x_2)^{n_2} \rangle \sim \left(\frac{L}{|x_2 - x_1|} \right)^{\tau_{n_1+n_2}} \left(\frac{|x_2 - x_1|}{\eta} \right)^{\tau_{n_1} + \tau_{n_2}} \tag{2}$$

also come with the same scaling [1]. It is not only the multifractal aspect of these models which is confirmed by the data [7], more subtle observed quantities like multiplier distributions [8–10] and Markovian Kramers-Moyal coefficients [11] have also been quantitatively reproduced by random multiplicative cascade processes [12–15]. But in spite of their success and inherent simplicity, random multiplicative cascade processes do have their drawbacks: at first there is no link to the fundamental Navier-Stokes equation and, secondly, no dynamics is included in these geometrical models as they are statically formulated in one-, sometimes in multi-dimensional spaces only. In this work we do not address the first problem, but present a solution for the second.

A dynamical generalisation of the geometric random multiplicative cascade processes is proposed, which is continuous and causal in space and time, and which generates positive-valued multifractal fields, like the energy-dissipation field of fully developed turbulence. This paper is an extension of Ref. [16] (see also [17]). The model construction is presented in Sect. II and relies on the multifractal scaling form (2) of two-point correlations only; stable statistics is used to facilitate analytical results. n-point correlations are discussed in Sect. III in the context of generalised fusion rules and are interpreted in terms of the random multiplicative weight picture of the geometric model precursors. Standard and non-standard observables, like integral moments and multiplier distributions are addressed in Sect. IV and shown to agree with data. Some model variations are presented in Sect. V.

II. MODEL-CONSTRUCTION BASED ON TWO-POINT CORRELATORS

A. Ansatz

For the positive-valued energy-dissipation field $\epsilon(x,t)$, depending on one space and time coordinate x and t, we assume a spatio-temporal multiplicative process,

$$\epsilon(x,t) = \exp\left\{ \int_{-\infty}^{\infty} dt' \int_{-\infty}^{\infty} dx' f(x-x', t-t')\, \gamma(x',t') \right\} \tag{3}$$

where $\gamma \sim S_\alpha((dxdt)^{\alpha^{-1}-1}\sigma, -1, \mu)$ is distributed according to a stable white-noise field [18]. The normalisation $\langle \epsilon(x,t) \rangle = \text{const} = 1$ determines the parameter $\mu = \sigma^\alpha / \cos(\pi\alpha/2)$. The symmetric index function

$$f(x,t) = \begin{cases} 1 & (0 \leq t \leq T,\ -g(T-t) \leq x \leq g(T-t)) \\ 0 & (\text{otherwise}) \end{cases} \tag{4}$$

is defined by the kernel-function $g(t)$; see Fig.1. Details of the explicit functional form for $g(t)$ will be derived in Sect. II.B. The energy-dissipation field $\epsilon(x,t)$ at spatio-temporal position (x,t) is composed multiplicatively of independent and identically distributed (*i.i.d.*) random-numbers $\exp\{\gamma(x,t)\}$, lying inside an attached domain, bounded by the kernel-function $g(t)$. The condition $0 \leq t \leq T$ for the index-function $f \neq 0$ ensures causality and defines the correlation-time T as the maximum of the temporal extension of the influence domain. L gives the maximum of the spatial extension and the correlation is given by $2g(0) = L$. With the locality-condition $g(T) = 0$, the influence domain is attached to the point (x,t) in an unequivocal way. These boundary conditions for the kernel-function $g(t)$ make the ansatz (3) a dynamical, causal and continuous process for the energy-dissipation field. This process is also homogeneous in space and time, as we assumed an *i.i.d* random-field $\gamma(x,t)$ and independence of the form of the influence domain from the spatio-temporal position.

The specification of the model is completed once the kernel-function $g(t)$ and the remaining parameters of the random-field $\gamma(x,t)$ are determined. This will be done in the next subsection where multifractal statistics is demanded from the ansatz (3). Technically two-point correlations will be employed for this derivation. Their geometrical structure is illustrated in Fig.2 for various spatio-temporal distances. We see that the correlation structure is a function of overlaps of influence domains, which on the other hand are bounded by the kernel-function $g(t)$. Thus two-point correlations give direct information about the kernel-function. Since we want to construct our process to produce a multifractal field, we first have to specify the interplay between two-point correlations and multifractality.

Multifractality of the energy-dissipation field $\epsilon(x,t)$ in fully developed turbulence [3] is usually observed by examining the scaling behaviour $\langle \overline{\epsilon}_l(x,t)^n \rangle \sim l^{-\tau_n}$ of the field amplitude $\overline{\epsilon}_l(x,t) = l^{-1}\int_{x-l/2}^{x+l/2} dx' \epsilon(x',t)$, coarse grained over a spatial domain of size l with centre x [7]; angular brackets denote the expectation value as the average over independent realizations of the field. Multifractality prevails once the scaling exponents τ_n are represented by polynomials in n, although often for given n, it is already difficult to unambiguously extract a unique value for τ_n via this standard route. Since the employed moments involve an integration over n-point statistics $\langle \epsilon(x_1,t)\cdots\epsilon(x_n,t)\rangle$, the latter are more fundamental to reveal multifractality. For example, an inertial range scaling $\left\langle \overline{\epsilon}_l^2(x,t)\right\rangle \sim l^{-\tau_2}$ of the second-order integral moment automatically implies the same scaling $\langle \epsilon(x,t)\epsilon(x+l,t)\rangle \sim l^{-\tau_2}$ for the two-point correlation; however the reverse need not be true [19,20].

For our purpose, we use two-point spatio-temporal correlators of arbitrary positive orders

$$r_{n_1,n_2}(\Delta x, \Delta t) = \frac{\langle \epsilon^{n_1}(x,t)\epsilon^{n_2}(x+\Delta x, t+\Delta t)\rangle}{\langle \epsilon^{n_1}(x,t)\rangle \langle \epsilon^{n_2}(x+\Delta x, t+\Delta t)\rangle}. \tag{5}$$

Spatio-temporal multifractality is incorporated by demanding scaling relations for the temporal and spatial two-point correlators

$$r_{n_1,n_2}(\Delta x = 0, \Delta t) \sim \Delta t^{-\tau[n_1,n_2]} \qquad (t_L \leq \Delta t \leq T - t_\eta) \tag{6}$$

$$r_{n_1,n_2}(\Delta x, \Delta t = 0) \sim \Delta x^{-\overline{\tau}[n_1,n_2]} \qquad (\eta \leq \Delta x \leq x_L) \tag{7}$$

with temporal and spatial multifractal scaling exponents $\tau[n_1,n_2]$ and $\overline{\tau}[n_1,n_2]$. For future purposes, we introduce arbitrary temporal $\Delta t \in [t_L, T - t_\eta]$ and spatial boundaries $\Delta x \in [\eta, x_L]$ for the scaling relations (6) and (7) to hold. One can think of $[\eta, x_L]$ as defining the inertial range for two-point correlators. Since we are dealing with a dynamical model, $[t_L, T - t_\eta]$ then defines a temporal inertial range.

B. Determination of the kernel-function g(t)

The multiplicativity of the process (3) with a stable white-noise field and the multifractal scaling of two-point correlators (6) and (7) are the only ingredients of our ansatz. The functional form of the kernel-function $g(t)$ will now be deduced solely out of these premises. Fig.2a illustrates the overlap of the influence domains of two points of the energy-dissipation field, having the same spatial position x but separated by a temporal distance Δt with $t_L < \Delta t < T - t_\eta$. Using the independence of $\gamma(x,t)$ at different spatio-temporal positions, the temporal two-point correlator (6) becomes

$$r_{n_1,n_2}(\Delta x = 0, \Delta t) = \frac{\left\langle \exp\left\{(n_1+n_2)\int_{V(\Delta t)} dx'dt'\gamma(x',t')\right\}\right\rangle}{\left\langle \exp\left\{n_1\int_{V(\Delta t)} dx'dt'\gamma(x',t')\right\}\right\rangle \left\langle \exp\left\{n_2\int_{V(\Delta t)} dx'dt'\gamma(x',t')\right\}\right\rangle}. \tag{8}$$

The influence domains of both points of the energy-dissipation field factorise into an overlap contribution $V(\Delta t)$ and two non-overlap contributions $V(0) - V(\Delta t)$. The latter appears in the denominator and the numerator of (5,) in the same respective orders n_1 and n_2 and cancel out. The remaining contributions are those from the overlap of the two influence domains. The overlap $V(\Delta t)$ is bounded by the kernel-function $g(t)$.

Using the Laplace-transform and the stable-property

$$\langle \exp\{\lambda_1\gamma_1 + \lambda_2\gamma_2\}\rangle = \exp\left\{\frac{-\sigma^\alpha}{\cos\left(\frac{\pi\alpha}{2}\right)}\left(\lambda_1^\alpha + \lambda_2^\alpha\right) + \mu\left(\lambda_1 + \lambda_2\right)\right\} \tag{9}$$

with *i.i.d.* $\gamma_1, \gamma_2 \sim S_\alpha(\sigma, -1, \mu)$ and $\lambda_1, \lambda_2 \geq 0$, together with $\lambda\gamma \sim S_\alpha(|\lambda|\sigma, \beta, 0)$ and $\gamma + \mu \sim S_\alpha(\sigma, \beta, \mu)$ for $\gamma \sim S_\alpha(\sigma, \beta, 0)$, after a straightforward calculation we get for the temporal correlators

$$r_{n_1,n_2}(\Delta x = 0, \Delta t) = \exp\left\{\frac{-\sigma^\alpha}{\cos\left(\frac{\pi\alpha}{2}\right)}\left((n_1+n_2)^\alpha - n_1^\alpha - n_2^\alpha\right)V(\Delta t)\right\}. \tag{10}$$

Eq. (10) is a purely geometrical relation connecting two-point statistics with overlapping domains. Since these overlap-domains are bounded by the kernel-function $g(t)$, the scaling relation (6) translates into

$$V(\Delta t) = \int_{\Delta t}^{T} dt' \int_{-g(t')}^{g(t')} dx' \sim \ln \Delta t \tag{11}$$

for $t_L \leq \Delta t \leq T - t_\eta$. Combining (11) with (6) and (10), the temporal scaling exponent then becomes $\tau[n_1, n_2] = a((n_1+n_2)^\alpha - n_1^\alpha - n_2^\alpha)$, with some constant a. Finally after differentiating (11) with respect to Δt, we get the kernel-function

$$g(t) = \frac{a_0}{t} \tag{12}$$

inside the temporal scaling regime $t \in [t_L, T - t_\eta]$, where $a_0 = \frac{a\cos\left(\frac{\pi\alpha}{2}\right)}{-2\sigma^\alpha}$. The singularity of $g(t)$ at $t \to 0$ and the condition of locality $g(T) = 0$ now justifies the introduction of the boundaries t_L and $T - t_\eta$ for the temporal scaling regime.

The scaling relation (6) is valid independent of the behaviour of $g(t)$ for $t > T - t_\eta$. This part of $V(\Delta t)$ in Fig. 2a is always a complete part of the overlap as long as $t_L \leq \Delta t \leq T - t_\eta$ and therefore contributes only as a constant prefactor. This gives the possibility to achieve locality $g(T) = 0$ with the arbitrary choice

$$g(t) = \frac{a_0}{t + \tilde{t}} - \frac{a_0}{T + \tilde{t}} \qquad (T - t_\eta \leq t \leq T), \tag{13}$$

where at $t = T - t_\eta$, $\tilde{t} = \sqrt{Tt_\eta - 7t_\eta^2/4} - T + t_\eta/2$ is fixed by continuity with (12). For $\tilde{t}$ real, we have to guarantee $T > 7t_\eta/4$. The reason for the specific choice (13) is simply to stay in the same class of polynomials of order -1 and to be able to give an analytical expression for the new constant $\tilde{t}$.

The temporal scaling behaviour is independent of the functional form of $g(t)$ for $0 \leq t \leq t_L$, as the intersection domain $V(\Delta t)$ is not bounded by $g(t)$ for $t < t_L$. This domain is fixed by the equal time two-point correlators

$$r_{n_1,n_2}(\Delta x, \Delta t = 0) = \frac{\left\langle \exp\left\{(n_1+n_2)\int_{V(\Delta x)} dx'dt'\gamma(x',t')\right\}\right\rangle}{\left\langle \exp\left\{n_1\int_{V(\Delta x)} dx'dt'\gamma(x',t')\right\}\right\rangle\left\langle \exp\left\{n_2\int_{V(\Delta x)} dx'dt'\gamma(x',t')\right\}\right\rangle}, \tag{14}$$

characterised by a spatial intersection domain $V(\Delta x)$ and calculated in the same way as for temporal correlators; consult again Fig. 2b. For simplicity the boundaries $\eta = 2g(T - t_\eta)$ and $x_L = 2g(t_L)$ of the scaling regime (7) are set equal to those of the temporal two-point correlators. Then the relation

$$2g(t(\Delta x)) = \Delta x \tag{15}$$

yields the intersection time $t(\Delta x)$, where the boundaries of the two domains of influence intersect with each other. Making use of (12), the spatial overlap reads

$$V(\Delta x) = \int_0^{t(\Delta x)} dt'(2g(t') - \Delta x) = 2\int_0^{t_L} dt' g(t') + 2a_0 \left(\ln \frac{2a_0}{\Delta x t_L} - 1 \right). \tag{16}$$

The simple choice

$$g(t) = \frac{2a_0}{t + t_L} \qquad (0 \le t \le t_L) \tag{17}$$

is not unique, but is acceptable as a simple continuous extension of (12) into the domain $0 \le t \le t_L$, leading also to the perfect scaling relation (7). Finally the cut-off t_L is fixed by the condition $g(0) = L/2$. The kernel-function $g(t)$ is completely specified by the scaling relations (6) and (7). It comes with the four parameters T, L, t_L, t_η, with the first two representing the correlation time and length and the latter two limiting the perfect scaling range of the two-point correlators. Note that by construction, the limit of the temporal scaling regime $t_\eta \neq 0$ is necessary for locality $g(T) = 0$ and avoids ultraviolet divergence in the spatial correlations. Two more parameters are hidden in the field construction (3) and enter via the stable white-noise field; these are the stable index α and the parameter a, determining the absolute strength of the multifractal scaling exponents. By adjusting to the experimentally observed scaling exponents $\tau[1,1] = \tau_2 = 0.225$ [4], one of them, say $a = 0.225/(2^\alpha - 2)$ becomes expressible in terms of the other. Fig. 1 shows the kernel-function $g(t)$ for parameters $\alpha = 1.9$ and $T = L = 2^8$, $t_L = t_\eta = 10$ in arbitrary units. Note again the three different functional forms for the kernel-function $g(t)$, the arbitrary small-scale contribution for $t > T - t_\eta$, the contribution $t_L \le t \le T - t_\eta$ responsible for scaling of temporal two-point correlators and the large scale contributions $t \le t_L$ responsible for the perfect scaling of spatial two-point correlators.

Independent of a special choice of parameters, the presented solution for $g(t)$ implies spatio-temporal equivalence of the scaling exponents

$$\overline{\tau}[n_1, n_2] = \tau[n_1, n_2] = a\left((n_1 + n_2)^\alpha - n_1^\alpha - n_2^\alpha\right). \tag{18}$$

This corresponds to the Taylor-Frozen-Flow Hypothesis [1] where correlations at a spatial distance are measured at a temporal distance. Here this hypothesis holds at least in the case of two-point correlations inside the scaling regime. Later on, it turns out that this is not true for arbitrary spatio-temporal n-point correlations.

C. Link to RMCP

In Ref. [16] the kernel-function $g(t)$ has been constructed in a different approach by linking the dynamical ansatz (3) directly to geometric random multiplicative cascade processes (RMCP). The functional form of the kernel-function $g(t)$ in [16] is more or less the same, differing only in the regimes $0 \le t \le t_L$ and $T - t_\eta \le t \le T$.

In a discrete RMCP the energy-dissipation

$$\epsilon(\eta) = \prod_{j=1}^{J} q(l_j) = \exp\left\{ \sum_{j=1}^{J} \ln q(l_j) \right\} \tag{19}$$

resolved at the dissipation scale η is given as the product of *i.i.d.* multiplicative weights $q(l_j)$ of a nested hierarchy of scales $\eta \le l_j = L'/\lambda^j \le L'$ with $\lambda > 1$. Comparing (19) with (3), the scale index j is replaced by a discrete time-index t_j with $2g(t_j) = l_j$, leading to

$$q(l_j) = \exp\left\{ \int_{t_{j-1}}^{t_j} dt' \int_{-g(t')}^{g(t')} dx' \gamma(x', t') \right\}. \tag{20}$$

Since $\gamma(x,t)$ is a stable white noise field, the independent multiplicative weights $q(l_j)$ become identically distributed once the volume associated to the time-strip integration, inside the exponential is scale-, i.e. j-independent. This leads directly to the result (12), valid for $t_L = g^{-1}(L'/2) \le t \le T - t_\eta$.

Identifying

$$\tilde{q}(L) = \exp\left\{ \int_0^{t_L} dt' \int_{-g(t')}^{g(t')} dt' \gamma(x', t') \right\} \tag{21}$$

and

$$\tilde{q}(\eta) = \exp\left\{\int_{T-t_\eta}^{T} dt' \int_{-g(t')}^{g(t')} dt' \gamma(x', t')\right\} \tag{22}$$

as large-scale and small-scale fluctuations, respectively, the field (3) can be written in the RMCP-analogue form

$$\epsilon(x,t) = \tilde{q}(\eta)\left(\prod_{j=1}^{J} q(l_j)\right)\tilde{q}(L), \tag{23}$$

where $J = \log_\lambda\left((T-t_\eta)/t_L\right)$ represents the number of discrete cascade steps.

Note that all $q(l_j)$ are *i.i.d.* for $1 \leq j \leq J$, whereas $\tilde{q}(\eta)$ and $\tilde{q}(L)$ come with different distributions. There is more analogy to geometric RMCP: in Ref. [21], it has been demonstrated that the experimentally motivated unrestrictive sampling of spatial two-point correlators leads to finite-size corrections to scaling, once the two-point distance approaches the integral length L and that this finite-size correction can be removed by a suitably tuned large-scale fluctuation. Since by construction, the dynamical RMCP (3) comes with perfect scaling for the two-point correlators (7), the large scale fluctuation $\tilde{q}(L)$ has to be viewed as perfectly tuned.

III. MORE ON N-POINT CORRELATIONS

A. Spatio-temporal two-point correlations

In the previous section we used only spatial and temporal correlations to fix the kernel-function $g(t)$. Now we examine arbitrary spatio-temporal two-point correlations $\langle\epsilon(x,t)\epsilon(x+\Delta x, t+\Delta t)\rangle$. It is straightforward to calculate these correlations as a function of the spatio-temporal overlap $V(\Delta x, \Delta t)$, which is shown as the shaded area in Fig. 2c. Analytical results however need a proper distinction of several cases, which depend on the relative position of the two space-time points. All can be treated analytically. Instead of presenting all these formulas, we prefer only to illustrate them with Fig.3. Fig.3a shows the two-point correlations as a function of Δt and Δx. Parameters are $\alpha = 1.9$, $\tau[1,1] = 0.225$ and in arbitrary units $t_L = 5$, $t_\eta = 1$, $T = L = 2^8$. For $\Delta x = 0$ a rigorous straight-line behaviour is observed in this log-log-log plot for $t_L \leq \Delta t \leq T - t_\eta$, which reflects the perfect scaling form of the limiting case (6). The same holds for the limiting case $\Delta t = 0$ in the range $\eta \leq \Delta x \leq x_L$; see again Eq. (7). As Δx and/or Δt increase, more and more deviations from the rigorous scaling behaviour can be seen. Once $\Delta x > L/2 + g(\Delta t) = L_{corr}(\Delta t)$, the two influence domains do not overlap any more and as a consequence decorrelation $\langle\epsilon(x,t)\epsilon(x+\Delta x \geq x + L_{corr}(\Delta t), t+\Delta t)\rangle = \langle\epsilon(x,t)\rangle\langle\epsilon(x+\Delta x, t+\Delta t)\rangle$ sets in. It is interesting to note that $L_{corr}(\Delta t)$ displays the functional form of the kernel-function $g(t)$.

B. Equal-time n-point correlations I

On our way to more complex correlation functions, equal time n-point correlations

$$\rho_n(x_1, m_1; \ldots; x_n, m_n) = \langle\epsilon(x_1,t)^{m_1}\cdots\epsilon(x_n,t)^{m_n}\rangle \tag{24}$$

of arbitrary order $m_1, \ldots, m_n$ are now investigated. First, we will reveal their general structure. In the two following subsections they will be discussed in the context of fusion rules [22] and generic RMCP structures. We restrict ourselves to equal-time correlations. The case of temporal correlations is straightforward and does not give any new insight. The more complicated inspection of arbitrary spatio-temporal n-point correlation functions is briefly touched in Subsect. III.E.

We again start with two points to exhibit the transition from two-point correlators to two-point correlation densities. Making use of (5) and the result (14), the equal-time two-point correlation density becomes:

$$\rho(x_1, m_1; x_2, m_2) = \langle\epsilon(x_1,t)^{m_1}\epsilon(x_2,t)^{m_2}\rangle$$

$$= r_{m_1,m_2}(|x_2 - x_1|, \Delta t = 0)\,\langle\epsilon(x_1,t)^{m_1}\rangle\,\langle\epsilon(x_2,t)^{m_2}\rangle$$

$$= \exp\left\{ \frac{\tau_2}{2a_0\left(2^\alpha - 2\right)} \left(\left(m_1^\alpha - m_1\right)\left(V_1/V_2\right) + \left(m_2^\alpha - m_2\right)\left(V_2/V_1\right) \right.\right.$$

$$\left.\left. + \left(\left(m_1+m_2\right)^\alpha - m_1 - m_2\right)\left(V_1 \cap V_2\right)\right)\right\}$$

$$= \overline{\rho}(m_1|V_1/V_2)\overline{\rho}(m_2|V_2/V_1)\overline{\rho}(m_1+m_2|V_1\cap V_2). \tag{25}$$

Here $V_i = \int_0^T dt \int_{-g(t)}^{g(t)} dx$ represents the volume of the influence domain, attached to point i. V_i/V_j represents volume V_i without the overlapping volume $V_i \cap V_j$ resulting from V_j. In Fig. 4a the volumes V_1/V_2, V_2/V_1 and $V_1 \cap V_2$ are labeled with their respective orders m_1, m_2 and $m_1 + m_2$; these three disjunct contributions fill the union of the two influence domains with no remaining overlaps and consequently factorise, leading to the last step of (25), where the abbreviation

$$\overline{\rho}(m|V) = \exp\left\{ \frac{\tau_2}{2a_0\left(2^\alpha - 2\right)} \left(m^\alpha - m\right) V \right\} \tag{26}$$

has been introduced.

For the third order $n = 3$ with points $x_1 < x_2 < x_3$, we arrive at the straightforward generalisation of (25)

$$\rho(x_1, m_1; x_2, m_2; x_3, m_3) = \overline{\rho}(m_1|V_1/V_2)\, \overline{\rho}(m_2|V_2/(V_1\cup V_3))\, \overline{\rho}(m_3|V_3/V_2)$$

$$\overline{\rho}(m_1+m_2|(V_1\cap V_2)/V_3)\, \overline{\rho}(m_2+m_3|(V_2\cap V_3)/V_1)$$

$$\overline{\rho}(m_1+m_2+m_3|V_1\cap V_2\cap V_3); \tag{27}$$

Consult Fig. 4b. For the most general case of an equal-time n-point correlation density with $x_1 < x_2 < \ldots < x_n$ we only state the result:

$$\rho(x_1, m_1; \ldots; x_n, m_n) = \prod_{j=1}^{n} \prod_{k=1}^{n-j+1} \overline{\rho}(m_k + \ldots + m_{k+j-1}|(V_k \cap \ldots \cap V_{k+j-1})/(V_{k-1} \cup V_{k+j})). \tag{28}$$

One gets contributions of all common histories of neighbouring points, first the contributions every point has non-overlapping with the others, second all contributions from overlaps with one neighbour, with two neighbours,... and finally one contribution of the overlap, all points have in common.

C. Equal-time n-point correlations II: generalised fusion rules

After presenting the overall structure of equal-time n-point correlation densities, in terms of the intuitive picture with disjunct contributions from different overlap volumes of the respective influence cones, we now aim to rewrite them in terms of a fusion-rule picture. Again, the focus is first on two-point, then on three- and four-point, and finally on n-point correlation densities.

Since the one-point moment $\langle \epsilon(x,t)^m \rangle$ is independent of the position x, the scaling behaviour of the equal-time two-point correlation density $\rho(x_1, m_1; x_2, m_2)$ is identical to the two-point correlator (7) for $\eta \leq \Delta x = x_2 - x_1 \leq x_L$. Hence we arrive at

$$\rho(x_1, m_1; x_2, m_2) \sim (x_2 - x_1)^{-\xi[m_1, m_2]} \tag{29}$$

with

$$\xi[m_1, m_2] = \frac{\tau_2}{2^\alpha - 2}\left(\left(m_1+m_2\right)^\alpha - m_1^\alpha - m_2^\alpha\right). \tag{30}$$

For our purposes it is instructive to rederive this result from the last line of (25). Noting that $\overline{\rho}(m|V_1/V_2) = \overline{\rho}(m|V_1)/\overline{\rho}(m|V_1\cap V_2)$ the scaling part of (25) is given by

$$\rho(x_1, m_1; x_2, m_2) \sim \frac{\overline{\rho}(m_1+m_2|V_1\cap V_2)}{\overline{\rho}(m_1|V_1\cap V_2)\overline{\rho}(m_2|V_1\cap V_2)}. \tag{31}$$

Realizing that $V_1 \cap V_2 = V(\Delta x = x_2 - x_1) \sim \ln \Delta x$ and making use of (26), Eq. (31) then transforms into Eq. (29).

In the expression (27) for the equal-time three-point correlator each of the six contributing factors is rewritten and then reordered, giving rise to

$$\begin{aligned}
&\rho(x_1, m_1; x_2, m_2; x_3, m_3) = \\
&= \frac{\overline{\rho}(m_1|V_1)}{\overline{\rho}(m_1|V_1 \cap V_2)} \, \frac{\overline{\rho}(m_2|V_2)\overline{\rho}(m_2|V_1 \cap V_3)}{\overline{\rho}(m_2|V_1 \cap V_2)\overline{\rho}(m_2|V_2 \cap V_3)} \, \frac{\overline{\rho}(m_3|V_3)}{\overline{\rho}(m_3|V_2 \cap V_3)} \\
&= \frac{\overline{\rho}(m_1 + m_2|V_1 \cap V_2)}{\overline{\rho}(m_1 + m_2|V_1 \cap V_3)} \, \frac{\overline{\rho}(m_2 + m_3|V_2 \cap V_3)}{\overline{\rho}(m_2 + m_3|V_1 \cap V_3)} \, \overline{\rho}(m_1 + m_2 + m_3|V_1 \cap V_3) \\
&\sim \frac{\overline{\rho}(m_1 + m_2|V_1 \cap V_2)}{\overline{\rho}(m_1|V_1 \cap V_2)\overline{\rho}(m_2|V_1 \cap V_2)} \, \frac{\overline{\rho}(m_2 + m_3|V_2 \cap V_3)}{\overline{\rho}(m_2|V_2 \cap V_3)\overline{\rho}(m_3|V_2 \cap V_3)} \, \frac{\overline{\rho}(m_1 + m_2 + m_3|V_1 \cap V_3)\overline{\rho}(m_2|V_1 \cap V_3)}{\overline{\rho}(m_1 + m_2|V_1 \cap V_3)\overline{\rho}(m_2 + m_3|V_1 \cap V_3)} \\
&\sim (x_2 - x_1)^{-\xi[m_1, m_2]} \, (x_3 - x_2)^{-\xi[m_2, m_3]} \, (x_3 - x_1)^{-\tilde{\xi}[m_1, m_2, m_3]} \, . \qquad (32)
\end{aligned}$$

The exponents $\xi[m_1, m_2]$ and $\xi[m_2, m_3]$ are the same as in (30), whereas the third one is now given by $\tilde{\xi}[m_1, m_2, m_3] = \frac{\tau_2}{2^\alpha - 2} \left((m_1 + m_2 + m_3)^\alpha - (m_1 + m_2)^\alpha - (m_2 + m_3)^\alpha + m_2^\alpha \right)$. The last line of (32) can be viewed as a generalised fusion rule; consult also Ref. [22].

The fusion rule (32) is easily generalised to arbitrary orders n. This is possible because all intersection domains can be written as a combination of $V_i \cap V_j \sim \ln |x_j - x_i|$, given that $\eta < |x_j - x_i| < x_L$ for all pairs of points. Proven by complete induction the equal-time n-point correlation density has the following structure:

$$\rho(x_1, m_1; \ldots; x_n, m_n) \sim \left(\prod_{i=1}^{n-1} (x_{i+1} - x_i)^{-\xi[m_i, m_{i+1}]} \right) \prod_{j=2}^{n-1} \prod_{l=j+1}^{n} (x_l - x_{l-j})^{-\tilde{\xi}[m_{l-j}, \ldots, m_l]} \, , \qquad (33)$$

where

$$\begin{aligned}
\tilde{\xi}[m_1, \ldots, m_i] &= \xi[m_1 + \ldots + m_{i-1}, m_i] - \xi[m_2 + \ldots + m_{i-1}, m_i] \\
&= \frac{\tau_2}{2^\alpha - 2} \left((m_1 + \ldots + m_i)^\alpha - (m_1 + \ldots + m_{i-1})^\alpha - (m_2 + \ldots + m_i)^\alpha + (m_2 + \ldots + m_{i-1})^\alpha \right) \qquad (34)
\end{aligned}$$

and $x_1 < x_2 < \ldots < x_n$ with $\eta < x_{i+1} - x_i < x_L$. The equal-time n-point correlation function factorises into contributions at the smallest scales $x_{i+1} - x_i$, next smaller scales $x_{i+2} - x_i$ ... and finally one contribution at the largest scale $x_n - x_1$. The first product in (33) gives the contributions from the smallest scales involving the scaling-exponents ξ and the second product counts all other scales with modified scaling exponents $\tilde{\xi}$. These modified scaling-exponents arise from the nested structure of the overlapping volumes.

D. Equal-time n-point correlations III: RMCP interpretation

So far the generalised fusion rule of the equal-time n-point correlation densities has been expressed in two ways: Eq. (33) uses relative distances between the involved points, whereas Eq. (28) employs overlap volumes of respective influence domains. Since already in Section II.C we interpreted the influence domains in terms of random multiplicative weights, it is natural to interpret the generalised fusion rules also in terms of random multiplicative weights. In order to simplify the presentation, small- and large-scale fluctuations (21) and (22) will be discarded.

Using the assignment (20) the expression (25) for the two-point correlation density can be expressed as

$$\rho(x_1, m_1; x_2, m_2) = \langle q^{m_1} \rangle^{j_1} \, \langle q^{m_2} \rangle^{j_2} \, \left\langle q^{m_1 + m_2} \right\rangle^{j_{1,2}} \, . \qquad (35)$$

In the RMCP language,

$$j_{1,2} = \frac{V_1 \cap V_2}{V_\lambda} \qquad (36)$$

with

$$V_\lambda = \int_{t_{j-1}}^{t_j} dt' \int_{-g(t')}^{g(t')} dx' = 2a_0 \ln \lambda. \tag{37}$$

denoting the number of steps the two points have evolved together during the cascade history and

$$j_1 = j_2 = \frac{V_1/\left(V_1 \cap V_2\right)}{V_\lambda} = \frac{V_2/\left(V_1 \cap V_2\right)}{V_\lambda} \tag{38}$$

represent the number of cascade steps the two points go through independently after their branching.

The three-point correlation density (27) displays the same structure:

$$\rho(x_1, m_1; x_2, m_2; x_3, m_3) = \langle q^{m_1} \rangle^{j_1} \langle q^{m_2} \rangle^{j_2} \langle q^{m_3} \rangle^{j_3} \left\langle q^{m_1+m_2} \right\rangle^{j_{1,2}} \left\langle q^{m_2+m_3} \right\rangle^{j_{2,3}} \left\langle q^{m_1+m_2+m_3} \right\rangle^{j_{1,2,3}}. \tag{39}$$

The first three factors constitute the multiplicative weights the three points do not have in common, the next two factors constitute the multiplicative weights which two of the three points have in common and finally the last line counts the multiplicative weights which all three points have in common. The numbers of multiplicative weights are given analogous to (36) and (38),

$$j_1 = \frac{V_1/V_2}{V_\lambda},\ j_2 = \frac{V_2/(V_1 \cup V_3)}{V_\lambda},\ j_3 = \frac{V_3/V_2}{V_\lambda} \tag{40}$$

$$j_{1,2} = \frac{(V_1 \cap V_2)/V_3}{V_\lambda},\ j_{2,3} = \frac{(V_2 \cap V_3)/V_1}{V_\lambda} \tag{41}$$

$$j_{1,2,3} = \frac{V_1 \cap V_2 \cap V_3}{V_\lambda}, \tag{42}$$

and are related to each other by

$$j_1 + j_{1,2} + j_{1,2,3} = j_2 + j_{1,2} + j_{2,3} + j_{1,2,3} = j_3 + j_{2,3} + j_{1,2,3}, \tag{43}$$

reflecting the total number of RMCP cascade steps. Higher order correlation densities are straightforward and result in the same structure of common multiplicative weights of all combinations of neighbouring points.

One more comment on the expression (39). In discrete RMCP, say with binary scale steps $\lambda = 2$, three points first share a common cascade history with $j_{1,2,3}$ steps. Then one point (say the third one) branches off and from then on evolves independently from the other two; consequently, $j_{2,3} = 0$ could be zero and $j_3 + j_{1,2,3}$ adds up to the total number of cascade steps. Only $j_{1,2}$ could be different from zero, since the first two points still share some more common cascade history; once those two branches, $j_1 = j_2$ independent steps are left until the RMCP evolution reaches the dissipation scale η. However, this RMCP result, i.e. $j_1 + j_{1,2} + j_{1,2,3} = j_2 + j_{1,2} + j_{1,2,3} = j_3 + j_{1,2,3}$, is not necessarily in conflict with the relation (43). The former reflects the ultrametric view of the nested hierarchy of RMCP length scales and is not observable for an experimentalist [12–15,21,23,24]. An unrestrictive sampling of discrete RMCP three-point correlations breaks the underlying ultrametric structure, leading to a modified result which may be closer to (43). This speculation should be tested with a discrete RMCP simulation. Definitely even more interesting would be to test the predicted generalised fusion rule structure (27), (32) and (39) of three-point correlations with data. Already the two-point correlations (2), (25), (29) and (35) are in excellent agreement with high Reynolds number data [25], but three-point correlations could represent an even more stringent model test.

E. Characteristic function

In this subsection, we conclude our discussions on n-point statistics and examine the most general space-time correlation-function $\langle \epsilon(x_1, t_1)^{\xi_1} \cdot \ldots \cdot \epsilon(x_n, t_n)^{\xi_n} \rangle$, containing all statistical information. It is equal to the generating function

$$Z[\xi(x,t)] = \left\langle \exp\left\{ \int_{-\infty}^{\infty} dx \int_{-\infty}^{\infty} dt\ \xi(x,t)\ \ln \epsilon(x,t) \right\} \right\rangle \tag{44}$$

for the logarithmic field, once $\xi(x,t) = \sum_{k=1}^{n} \xi_k \delta(t - t_k) \delta(x - x_k)$ is chosen. The determination of Z is easily performed by regarding (44) as a summation of *i.i.d.* stable-distributions $\gamma(x,t)$ integrated over their influence domain:

$$Z[\xi(x,t)] = \left\langle \exp\left\{ \int_{-\infty}^{\infty} dx' \int_{-\infty}^{\infty} dt' \gamma(x',t') V_\xi(x',t') \right\} \right\rangle$$

$$= \exp\left\{ \frac{\sigma^\alpha}{\cos\left(\frac{\pi\alpha}{2}\right)} \int_{-\infty}^{\infty} dx' \int_{-\infty}^{\infty} dt' \left(V_\xi(x',t') - V_\xi^\alpha(x',t') \right) \right\}. \tag{45}$$

The first line is the result of inserting Eq. (3) into (44); also the abbreviation

$$V_\xi(x',t') = \int_{-\infty}^{\infty} dx \int_{-\infty}^{\infty} dt f(x-x', t-t') \xi(x,t) \tag{46}$$

has been introduced. For the second step of (45), the Laplace transform of stable distributions has been used. The result (45) is very convenient for numerical implementation: for n-point correlation densities $\langle \epsilon(x_1,t_1)^{\xi_1} \dots \epsilon(x_n,t_n)^{\xi_n} \rangle$ the test function $\xi(x,t) = \sum_{k=1}^n \xi_k \delta(x-x_k)\delta(t-t_k)$ is a weighted sum of δ-functions, so that (46) simply counts the number of weighted spatio-temporal points inside the influence domain attached to (x',t'). Note also, that the modified n-point correlation densities $\langle (\ln \epsilon(x_1,t_1))^{m_1} \cdots (\ln \epsilon(x_n,t_n))^{m_n} \rangle$, which follow from (44) by taking functional derivatives with respect to $\xi(x,t)$, only exist for the lowest orders, once $\alpha \neq 2$ is chosen for the random field $\gamma(x,t)$.

IV. COARSE GRAINED OBSERVABLES

In this Section, we examine statistical properties of coarse grained observables like integral moments and multiplier distributions. These are representative observables for the analysis of the experimentally measured surrogate energy dissipation field of fully developed turbulence.

A. Integral moments

The temporal integral moments of order n are defined as the expectation value of the coarse-grained temporal average of the energy-dissipation field

$$M_t^{(n)}(x_0,t_0) = \frac{1}{t^n} \left\langle \left(\int_{t_0-t/2}^{t_0+t/2} dt' \epsilon(x_0,t') \right)^n \right\rangle \sim \left(\frac{T}{t}\right)^{\tau_t(2)}. \tag{47}$$

Within the inertial range of fully developed turbulence these moments show multifractal scaling with exponent $\tau_t(n)$ [4]. Spatial integral moments, together with spatial scaling exponents $\tau_x(n)$ are defined as the coarse grained spatial average of the energy-dissipation field. Invoking the Taylor-Frozen-Flow Hypothesis [1], the spatial scaling exponents are believed to coincide with their temporal counterparts. For the time being, we present analytical model results for the temporal coarse graining and show numerical results for the spatial case.

Integral moments of order n involve an integration over all n-point correlations. This integration can be done by integrating the second-order correlation function (5) with $n_1 = n_2 = 1$:

$$M_t^{(2)}(x_0,t_0) = c_2 \left(\frac{t_L}{t}\right)^2 + c_1 \left(\frac{t_L}{t}\right) + c \left(\frac{T-t_\eta}{t}\right)^{\tau_2}$$

for $t_L \leq t \leq T - t_\eta$. The exponent $\tau_2 = a(2^\alpha - 2)$ should be set equal to the experimentally accepted value of 0.225 [4]. For $t_L \ll t \ll T - t_\eta$ the last term $\sim t^{-\tau_2}$ dominates the second-order integral moment, so that $M_t^{(2)}(x_0,t_0) \sim t^{-\tau_2}$ for intermediate scales. The analytic expressions for the coefficients c, c_1 and c_2 are:

$$c = 2\exp\left\{ \frac{\tau_2}{2a_0} V(T-t_\eta) \right\} \left(\frac{1}{1-\tau_2} - \frac{1}{2-\tau_2} \right) \tag{48}$$

$$c_1 = 2 \left\{ \frac{\exp\left\{\frac{\tau_2}{2a_0} V(t_L)\right\}}{1-2\tau_2} \left(2 - 2^{2\tau_2}\right) - \frac{\exp\left\{\frac{\tau_2}{2a_0} V(T-t_\eta)\right\} (T-t_\eta)^{\tau_2} t_L^{-\tau_2}}{1-\tau_2} \right\} \tag{49}$$

$$c_2 = 2 \left\{ \frac{\exp\left\{\frac{\tau_2}{2a_0} V(t_L)\right\}}{1-2\tau_2} \left(-\frac{2^{2\tau_2}}{2-2\tau_2} + \frac{4}{2-2\tau_2} - 2 \right) + \frac{\exp\left\{\frac{\tau_2}{2a_0} V(T-t_\eta)\right\} (T-t_\eta)^{\tau_2} t_L^{-\tau_2}}{2-\tau_2} \right\} \tag{50}$$

with the $V(t)$-expressions given by (11). The determination of higher order moments is straightforward, though cumbersome.

Fig. 5 shows the local slope of $\log M^{(n)}$ as a function of the average domain $\log t$ and $\log l$ for the temporal (Fig. 5a) and the spatial integral moments (Fig. 5b), respectively. Parameters have been set $\alpha = 1.9$ and in arbitrary units $t_L = 5t_\eta = 5$, $T = L = 2^8$. For very small and very large scales there are weak deviations from perfect scaling, which increase as the order n increases. Comparing the temporal and spatial local slopes, there is clearly a larger scaling regime for the spatial moments. This is a result of the small scale statistics where temporal and spatial two-point correlations show a different behaviour. Once again, the message is that it is better to use two-point correlators instead of integral moments to extract multifractal scaling exponents.

B. Multiplier-pdf

Having examined moments of coarse-grained observables in the previous subsection, we now investigate the probability density function $p(M)$ of ratios of these observables, the so-called multipliers:

$$M_x(x,t,l_x) = \frac{\int_{x-l_x/2}^{x} \epsilon(x',t)dx'}{\int_{x-l_x/2}^{x+l_x/2} \epsilon(x',t)dx'},$$
$$M_t(x,t,l_t) = \frac{\int_{t-l_t/2}^{t} \epsilon(x,t')dt'}{\int_{t-l_t/2}^{t+l_t/2} \epsilon(x,t')dt'}. \tag{51}$$

Here we have only displayed the definition of a left-sided spatial and temporal multiplier M_x and M_t, respectively, where the daughter domain of size $l/2$ is located at the left of the mother domain of size l. In the same manner right-shifted or centered multipliers, also with other scale steps, can be defined. A series of experimental investigations [8,10] for large Reynolds number turbulent flows resulted in a β-distribution with $\beta \sim 3.2$ for the left multiplier-distribution, scale-independent in the upper part of the inertial range. The most important result is reflected in the conditional multiplier distributions $p(M(l)|M(2l))$ [8], where correlations among multipliers with nested coarse graining domains at nearby scales have been observed: compared to the unconditioned pdf, for the left/right-sided multipliers one gets a more narrow pdf, if conditioned on a small parent multiplier and a more broader pdf, if conditioned on a large parent multiplier. On first view, the conditioning effects violate the assumptions of RMCPs since those require *i.i.d.* random-weights $q(l)$. However, the contradiction is resolved once the observationally unavoidable unrestrictive sampling and the assumption of a nonconservative cascade generator is taken into account within the simple RMCPs [12,13]. Since we pointed out that our dynamical approach can be viewed as a generalisation of these successful models, we now ask, for the outcome of these unconditioned and conditioned multiplier pdfs within the dynamical cascade model.

We also report the differences between spatial and temporal multiplier distributions. The results presented here rely on simulations. Model parameters have been set $\tau[1,1] = 0.225$, $\alpha = 1.92$ and in arbitrary units $T = L = 2^8$, $t_\eta = t_L = 1$. The kernel-domain has been discretized into cells of size $dt = 0.1$, $dx = 0.1$, each filled with one random number γ. Stability of the results with respect to cell size and the number of independent samples of the energy-dissipation field has been checked. Fig. 6 shows (a) the temporal and (b) the spatial multipliers (51) obtained from 10^5 field samples. For comparison the β distribution with $\beta = 3.2$ is depicted as the solid line.

The unconditioned left-sided temporal multiplier-distribution is well-fitted by the experimentally observed β-distribution, if the index of stability α is set equal to 1.92. For larger α all distributions become slightly more narrow and for smaller α they become slightly broader. Also the correct scale-correlations are reproduced in the conditioned distributions. These pdf's are scale invariant for $l_t > 2^{-4}T$, that is over four binary orders of magnitude. For smaller scales all distributions become broader. The qualitative behaviour of temporal multiplier distributions remains unchanged once spatial multipliers are examined. But there is a clear quantitative difference, all spatial multiplier distributions are a little broader compared to their temporal counterpart. The differences arise again from the different small and large scale behaviour of n-point correlations. Scale independence and conditioning effects are nevertheless not affected. These model simulations demonstrate that the proposed spatio-temporal cascade process is also able to reproduce the experimental multiplier findings.

V. MODEL GENERALISATION TO $3+1$ DIMENSIONS

So far the dynamical cascade process has been formulated in $1+1$ dimensions. Generalisations to $n+1$ dimensions are straightforward. Their construction again relies on the scaling properties of spatial and temporal two-point correlators. In the following we only state the results for the special case $n=3$ where the boundary conditions yield the most simplest analytical relations:

Sticking to spherical symmetry, the kernel function $g(t)$ of $1+1$ dimensions is replaced by the time-dependent radius $r(t)$, so that the scalar field $\epsilon(\vec{r},t)$

$$\epsilon(\vec{r},t) = \exp\left\{\int_{t-T}^{t} dt' \int_{B^{(3)}_{r(t'-t+T)}(\vec{r})} d\vec{r'}\gamma(\vec{r'},t)\right\} \tag{52}$$

is then composed of time-dependent 3-dimensional balls $B^{(3)}_{r(t)}(\vec{r})$. Scaling relations for spatial and temporal two-point correlators with symmetric scaling exponents $\overline{\tau}=\tau$ immediately imply

$$r(t) = \begin{cases} \left(\frac{a_0}{t+\tilde{t}} - \frac{a_0}{T+\tilde{t}}\right)^{\frac{1}{3}} & T-t_\eta \le t \le T \\ \left(\frac{a_0}{t}\right)^{\frac{1}{3}} & t_L \le T-t_\eta \\ \frac{a_0^{1/3}}{(t+t_0)^\xi} & 0 \le t \le t_L \end{cases} . \tag{53}$$

The functional form for $t > T-t_\eta$ again is arbitrary and only affects a constant prefactor in the temporal scaling. The functional form for $t_L \le t \le T-t_\eta$ is fixed by the temporal scaling prerequisite $V(\Delta t) \sim \ln \Delta t$. The new parameters ξ and t_0 are fixed by two boundary conditions, continuity at $t=t_L$ and a spatial scaling relation $V(\Delta x) \sim \ln \Delta x$:

$$\begin{aligned} t_L^{2\xi-2/3} &= \frac{\left(\frac{t_0}{t_L}+1\right)^{1-2\xi} - \left(\frac{t_0}{t_L}\right)^{1-2\xi}}{3(1-2\xi)}, \\ t_L &= (t_0+t_L)^{3\xi} . \end{aligned} \tag{54}$$

The choice $\xi=2$, for example results in $t_L \sim 0.33$ and $t_0 \sim 0.5$. Of course, other choices of ξ are also possible.

VI. CONCLUSION

The dynamical model presented here is constructed from a strict multifractal scaling of two-point correlators and employs stable statistics of the random-field γ. The latter allows an analytical treatment of n-point correlations. For fully developed turbulence, the dynamical model is not only able to reproduce the observed multifractal scaling of two-point correlators for the energy dissipation field, but also the observed multiplier distributions, including scale-correlations. The dynamic model also predicts specific generalised fusion rules for n-point correlations; experimentally the sampling of at least three-point correlations should be feasible and could represent an even more stringent test of the proposed model. Another interesting observable, to be discussed in future, are n-point cumulants of logarithmic field amplitudes [24]. In this context, it might be necessary to formulate the proposed continuous dynamical model in a discrete way, introducing smallest spatio-temporal cells of size of the order of the dissipation scale and thus allowing to include deviations from log-stable statistics.

Already in the last Section, we have sketched the formulation of the dynamical model in $3+1$ dimensions. The extension to arbitrary $n+1$ dimensions is straightforward. Other generalisations in $n+1$ dimensions would be to include spatial anisotropy and boundary layer effects; work in this direction is already in progress [26]. As possible applications of the proposed dynamical cascade model, we see simulations for the spatio-temporal evolution of multifractal fields like rain and cloud fields in geophysics. In a numerically improved way, it might even serve as an efficient model generator for the turbulent small scale motion entering large-eddy simulations and other numerical approaches.

ACKNOWLEDGMENTS

The authors acknowledge fruitful discussions with Hans C. Eggers. This work has been supported in parts by DAAD.

[1] A.S. Monin and A.M. Yaglom, *Statistical Fluid Mechanics*, Vols. 1 and 2, (MIT Press, Cambridge, 1971).
[2] A.N. Kolmogorov, Dokl. Akad. Nauk. SSSR **32**, 16 (1941).
[3] U. Frisch, *Turbulence*, (Cambridge University Press, Cambridge, 1995).
[4] K.R. Sreenivasan and R.A. Antonia, Ann. Rev. Fluid Mech. **29**, 435 (1997).
[5] T. Bohr, M.H. Jensen, G. Paladin and A. Vulpiani, *Dynamical systems approach to turbulence*, (Cambridge University Press, Cambridge, 1998).
[6] L.F. Richardson, *Weather prediction by numerical process*, (Cambridge University Press, Cambridge, 1922).
[7] C. Meneveau and K.R. Sreeenivasan, J. Fluid Mech. **224**, 429 (1991).
[8] K.R. Sreenivasan and G. Stolovitzky, J. Stat. Phys. **78**, 311 (1995).
[9] J. Molenaar, J. Herweijer and W. van de Water, Phys. Rev. E **52**, 496 (1995).
[10] G. Pedrizzetti, E.A. Novikov and A.A. Praskovsky, Phys. Rev. E **53**, 475 (1996).
[11] A. Naert, R. Friedrich, and J. Peinke, Phys. Rev. E **56**, 6719 (1997).
[12] B. Jouault, P. Lipa, and M. Greiner, Phys. Rev. E **59**, 2451 (1999).
[13] B. Jouault, M. Greiner, and P. Lipa, Physica D **136**, 125 (2000).
[14] B. Jouault, J. Schmiegel, and M. Greiner, chao-dyn/9909033.
[15] J. Cleve and M. Greiner, Phys. Lett. A **273**, 104 (2000).
[16] J. Schmiegel, H. C. Eggers and M. Greiner, preprint cond-mat/0106347.
[17] F. Schmitt and D. Marsan, preprint cond-mat/0102346.
[18] G. Samarodnitzky and M. Taqqu, *Stable non-Gaussian random processes* , (Chapman & Hall, New York, 1994).
[19] M. Greiner, J. Giesemann, P. Lipa and P. Carruthers, Z. Phys. C **69**, 305 (1996).
[20] M. Wolf and M. Greiner, Phys. Lett. A **266**, 276 (2000).
[21] J. Schmiegel, T. Dziekan, J. Cleve, B. Jouault and M. Greiner, preprint *Scaling functions in a random multiplicative energy-cascade model of turbulence*.
[22] V. L'vov and I. Procaccia, Phys. Rev. Lett. **76**, 2898 (1996).
[23] M. Greiner, J. Giesemann und P. Lipa, Phys.Rev. E56 4263 (1997).
[24] H.C. Eggers, T. Dziekan and M. Greiner, Phys. Lett. A **281**, 249 (2001).
[25] T. Dziekan,"Zwei-Punkt-Kumulanten in synthetischer Turbulenz", diploma thesis (TU Dresden, 2001); T. Dziekan, J. Cleve and K.R. Sreenivasan, private communication.
[26] J. Schmiegel and M. Greiner, in preparation.

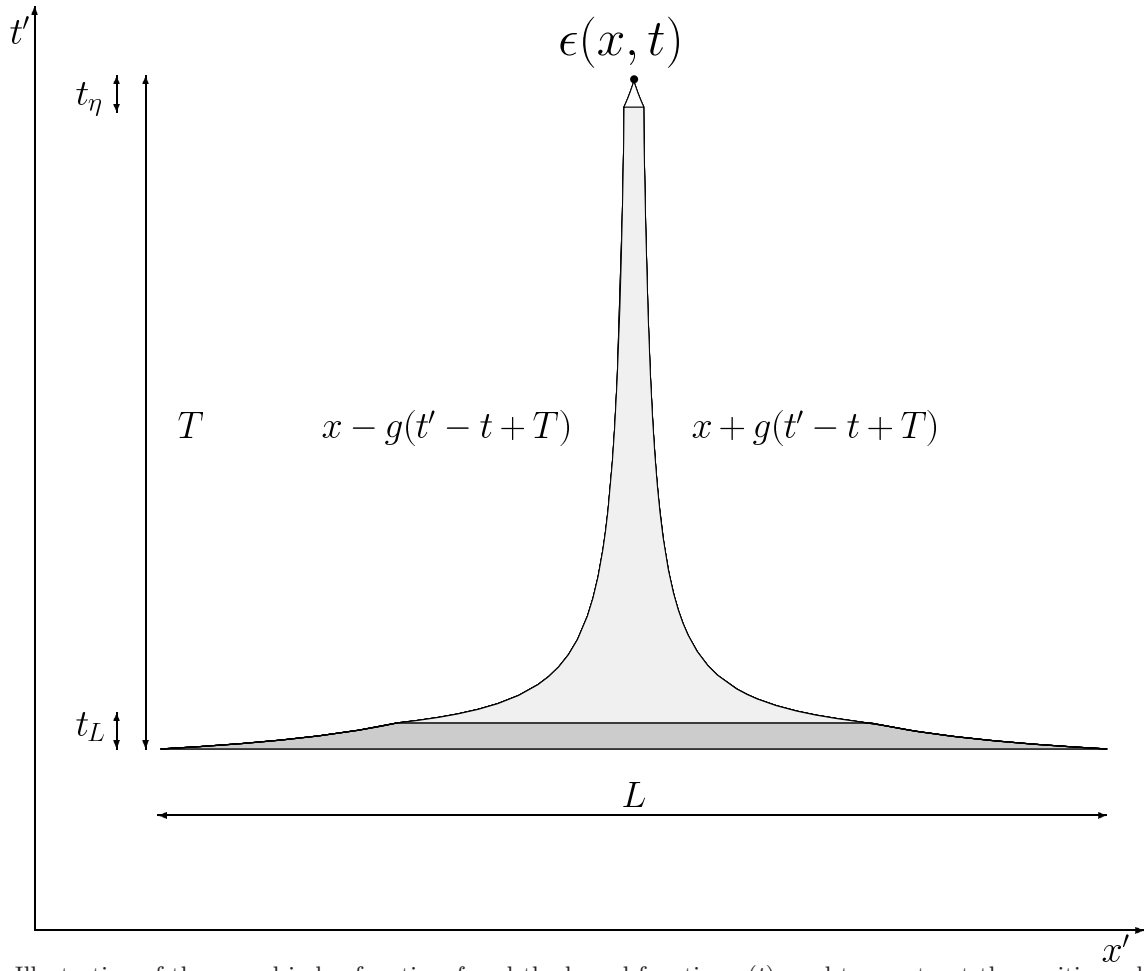

FIG. 1. Illustration of the causal index function f and the kernel function $g(t)$ used to construct the positive-valued multifractal field $\epsilon(x,t)$.

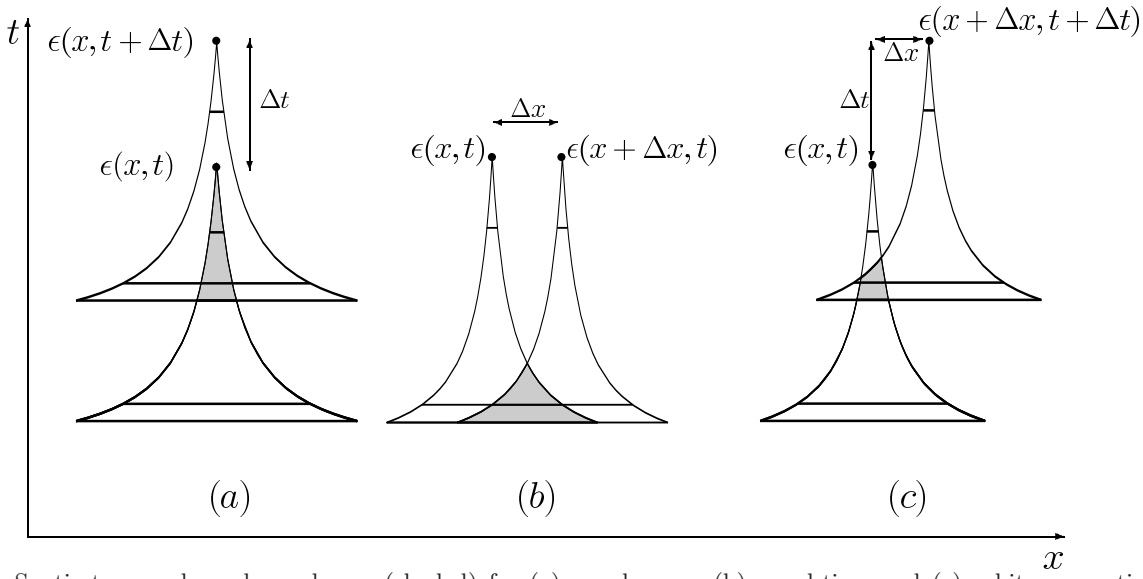

FIG. 2. Spatio-temporal overlap volumes (shaded) for (a) equal-space, (b) equal-time and (c) arbitrary spatio-temporal distance.

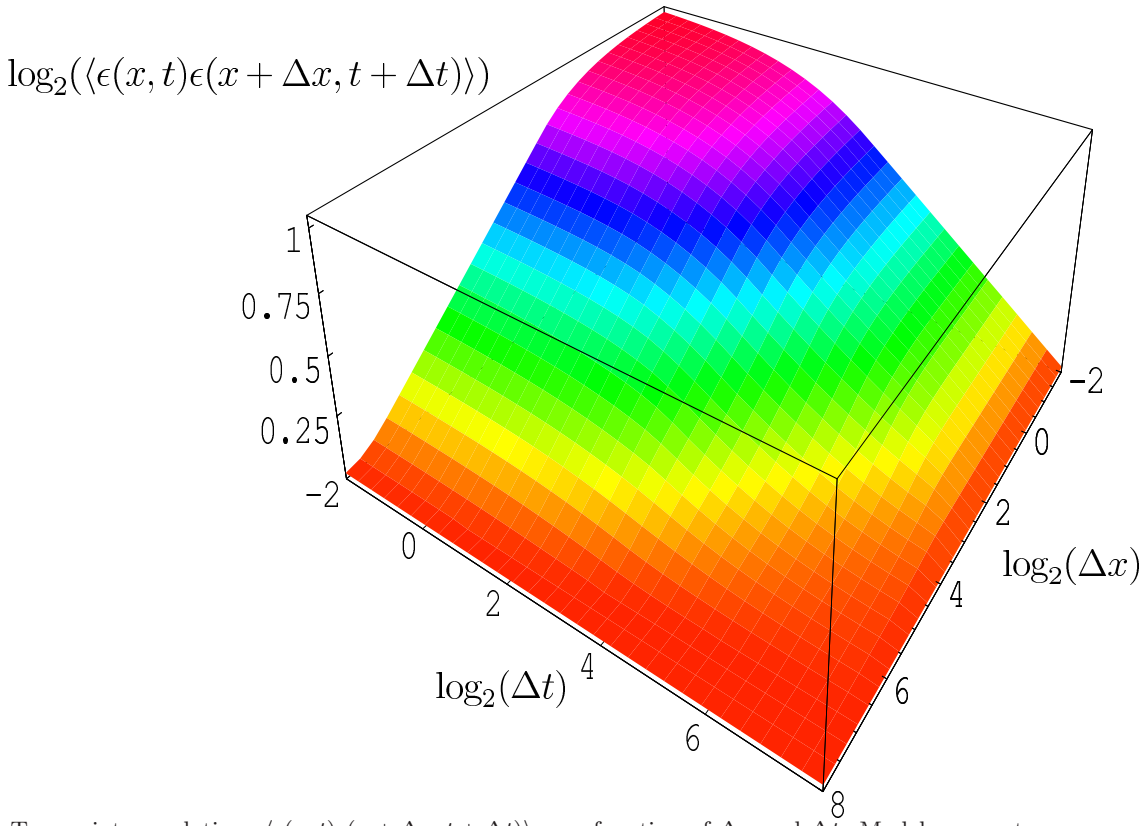

FIG. 3. Two-point correlations $\langle\epsilon(x,t)\epsilon(x+\Delta x,t+\Delta t)\rangle$ as a function of Δx and Δt. Model parameters are quoted in the text.

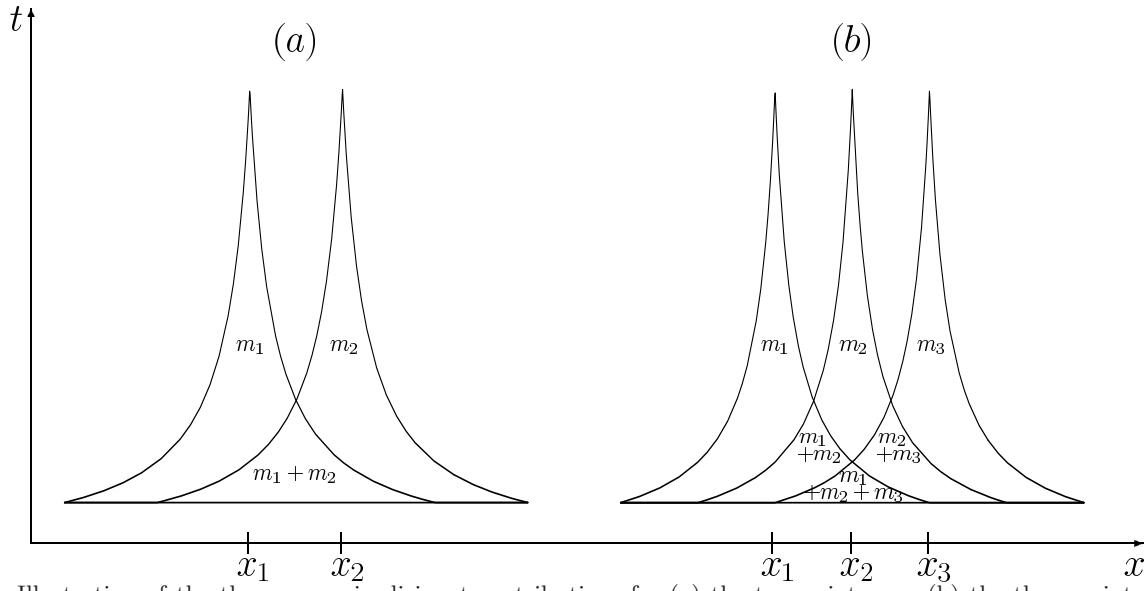

FIG. 4. Illustration of the three resp. six disjunct contributions for (a) the two-point resp. (b) the three-point equal-time correlation density.

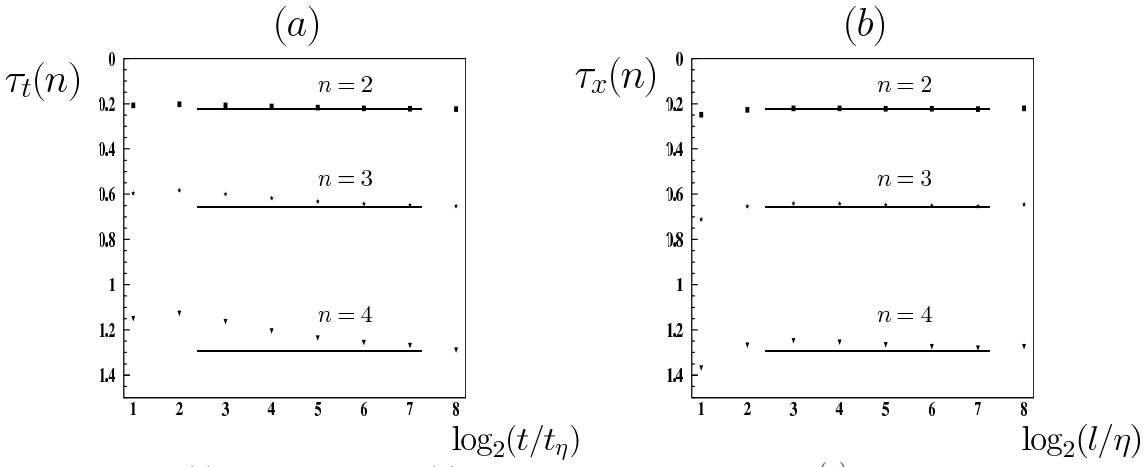

FIG. 5. Local slopes of (a) the temporal and (b) the spatial integral moments $M^{(n)}$ of order $n = 2, 3, 4$ as a function of the coarse-graining scale t and l, respectively. Model parameters are quoted in the text. For comparison the two-point scaling exponents $\tau_n = 0.225(n^\alpha - n)/(2^\alpha - 2)$ are indicated by straight lines.

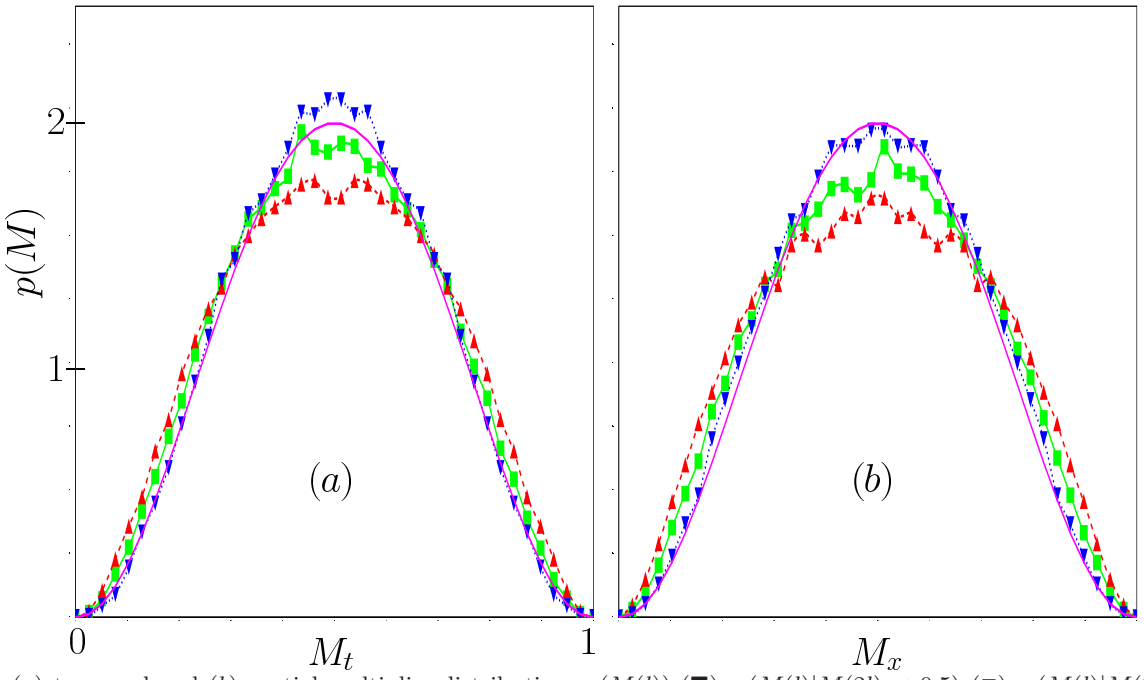

FIG. 6. (a) temporal and (b) spatial multiplier-distributions $p(M(l))$ (■), $p(M(l)|M(2l) < 0.5)$ (▼), $p(M(l)|M(2l) > 0.5)$ (▲) for $t = T/8$ and $l = L/8$. Model parameters as quoted in the text.